Hydrodynamic instability seeding by oxygen nonuniformities in glow discharge polymer inertial fusion ablators

S. J. Ali, P. M. Celliers, S. W. Haan, T. R. Boehly, N. Whiting, S. H. Baxamusa, H. Reynolds,
M. A. Johnson, J. D. Hughes, B. Watson, K. Engelhorn, V. A. Smalyuk, and O. L. Landen

Hydrodynamic instability seeding by oxygen nonuniformities in glow discharge polymer inertial fusion ablators

S. J. Ali,[1] P. M. Celliers,[1] S. W. Haan,[1] T. R. Boehly,[2] N. Whiting,[2] S. Baxamusa,[1] H. Reynolds,[3] M. A. Johnson,[1] J. D. Hughes,[1] B. Watson,[3] K. Engelhorn,[3] V. A. Smalyuk[1], O. L. Landen[1]

1) Lawrence Livermore National Laboratory, 7000 East Avenue, Livermore, California 94550, USA
2) Laboratory for Laser Energetics, University of Rochester, 250 East River Road, Rochester, New York 14623, USA
3) General Atomics, 3550 General Atomics Court, San Diego, California 92121, USA

Abstract

The U.S. indirect drive inertial confinement fusion (ICF) program uses glow discharge polymer (GDP) as the one of the ablator materials for the ICF experiments on the National Ignition Facility (NIF). The performance of those implosions using may be adversely affected by photoactivated uptake of oxygen impurities in the surface of GDP ablator. These impurities can induce significant perturbations in the shockwaves generated in the ablator. These perturbed shocks generate mass modulations that are amplified by Rayleigh-Taylor (RT) instability and reduce the performance of the implosions. Here we report on experiments that provide a quantitative connection between photoactivated oxygen uptake in GDP samples and modulations in shock velocities in the samples. The observed shock nonuniformity confirms the hypothesis that irregular oxygenation is a competent seed for the RT and can have a significant effect on NIF GDP implosions.

The goal of the inertial confinement fusion research is to create laboratory-scale fusion burn of deuterium-tritium fuel using spherical compression combined with central hot-spot heating [1,2]. Current designs contain a frozen DT fuel layer inside a hollow, spherical capsule made of a low atomic number material. Three candidate capsule materials are being explored on the National Ignition Facility [3]: beryllium [4], high-density carbon [5], and an amorphous hydrogenated carbon referred to as glow discharge polymer, or GDP [6]. In the indirect drive scheme the capsule surface is ablated by a radiation drive of soft x-rays generated by the laser irradiation of the interior walls of a surrounding cavity [1]. The implosion process is unstable, due to Rayleigh-Taylor amplification of perturbations at the ablation surface and the interior surfaces of the shell [1,7]. Current designs undergo perturbation growth factors of 100 to 1000 depending on the design and perturbation wavelength, thus a high degree of capsule uniformity is essential to maintain shell integrity by the end of the implosion [8,9]. Modeling of the implosions has focused on several known instability seeds, such as: the surface roughness [1,7,10-12], the capsule supporting structure [13-15] and the fill tube [16]. Degradation in current GDP implosions is predicted to be dominated by the capsule support structure and irradiation asymmetry [12]. As these perturbations are reduced, the surface roughness and, as discussed here, composition nonuniformities will become increasingly important. Experimental evidence for the presence of additional seeds in GDP capsules, in the form of larger-than-expected in-flight modulations and coherent features, was found in experiments that observe in-flight uniformity [17]. An analysis by Haan et al. [12,18,19] suggested that nonuniformities in the oxygen content at the capsule surface could be a more significant seed for hydrodynamic instabilities than typical surface roughness. In the other ablators, shock propagation in the bulk is thought to introduce hydrodynamic irregularities due to the polycrystallinity and complex microstructure [20,21], but these processes are generally thought not to apply to the more amorphous GDP ablators at Mb shock pressures.

GDP capsules are fabricated via plasma chemical vapor deposition [6,22]. While most polymer materials require UV light to photoexcite the electrons and induce reaction, GDP photo-oxidizes at wavelengths as long as 530 nm [23]. It has been confirmed by Baxamusa et al. [24] and Huang et al. [25] that the light exposure experienced by the target during normal fabrication processes can introduce measurable variations in the surface oxygen concentration [24]. The additional oxygen is primarily in the form of carbonyl and hydroxyl groups that replace existing CH bonds and form carboxylic acid groups, although there is evidence for the formation of additional byproducts that could not be identified [24]. To a good approximation the density of the material increases accordingly. This oxygen seed can induce Rayleigh-Taylor instability growth primarily through the

resulting variations in the soft-x-ray opacity. In the region with more oxygen, the higher opacity material reradiates more of the absorbed x-ray energy, resulting in less net absorption and lower ablation pressure. A region of GDP that has been perturbed with 1 at-% additional oxygen will produce 0.7% lower local ablation pressure during the production of the first shock of the implosion. The vorticity introduced by this seed propagates throughout the capsule and fuel and seeds the late stage RT growth.

Here we report experiments designed to quantify the magnitude of the effect of oxygen heterogeneities on shock waves in GDP driven by the Omega-60 laser facility at the Laboratory for Laser Energetics [26]. Two-dimensional laser velocimetry is used to measure modulations in shock fronts that are produced by variations in oxygen content deliberately imposed in planar GDP samples. The target design, shown in Fig. 1(a), consists of a 2 mm long by 3 mm diameter hohlraum irradiated with 2.3 kJ of 0.35 μm light through a single laser entrance hole (LEH) of 1.8 mm diameter. A 35-50 μm thick GDP ablator sample, mounted over a hole opposite to the LEH, was thermally bonded to a 40-60 μm poly(methyl methacrylate) (PMMA) layer and then epoxied to a 750 μm fused silica window with an external anti-reflection coating. The 3 ns reverse-ramp 15-beam laser drive heats the hohlraum to about 90eV, resulting in a peak pressure in the GDP of 2.2 Mbar, close to the pressure of the first shock in the multi-stage NIF ICF compression path. An additional five beams began at 2.8 ns to maintain a steady radiation drive for the shock wave over the experimental duration of 4 ns.

Controlled preparation of oxygen modulations photo-induced in the GDP samples was achieved by irradiating the foils with 400-nm light from a blue light-emitting diode light source through a periodic mask, to produce the oxygenation pattern [27]. A 100 μm period oxygen pattern was imprinted on the drive side of the GDP ablator prior to bonding to the PMMA [27]. Targets without oxygen patterning were also prepared. In all cases the targets were carefully protected from unnecessary light exposure during assembly and transportation. The oxygen modulation produces both density and opacity variations across the spatial extent of the sample. During the ablation process this pattern is transferred to the shock front produced in the GDP and propagates through the target and these modulations on the optically reflective shock front were detected using the two-dimensional Omega High-Resolution Velocimeter [28]. The PMMA layer is required as a witness layer for the optical diagnostic because GDP is opaque to the 400 nm wavelength probe beam, while PMMA is transparent. Measurements are taken once the shock enters the PMMA.

The spatial distribution of the oxygen impurity was determined using phase-shifting diffraction interferometry (PSDI) which measures variations in the optical path difference (OPD) through the GDP foil [29,30]. The oxygen concentration at selected locations in the foil was determined using Fourier transform infrared resonance (FTIR) as in Ref. [27] and the depth profile was determined using secondary ion mass spectrometry (SIMS) at various depths in the foil. The oxygen profile vs depth is approximately linear, from the maximum of ~12 at. % at the surface as shown in Fig. 1(b) and (c), down to a bulk level of 1 at. % at depths beyond 2 μm. This depth corresponds to the absorption depth for the 400-nm light used to create the oxygen perturbations. For the modulated samples discussed below, the oxygen concentration difference averaged through a 50 μm foil was 0.101 ± 0.024 at. %. The masked exposure protocol also resulted in surface topography modulations with a shape like the oxygen atomic percent line out shown in Fig. 1(c) and peak-to-valley amplitude of 35 nm. Separate ellipsometry measurements on submicron foils by one of us (S.H.B.) established that adding oxygen to GDP decreases its refractive index, and provided curves of density and refractive index vs oxygenation. The best agreement with all the characterization data is achieved by using this density vs oxygenation curve, and assuming that the refractive index is linear with oxygen concentration, with slope 0.003 refractive index change per at. % oxygen. The detailed model used for simulating the experiments uses the depth profile from the FTIR, the overall oxygen amounts as determined from secondary ion mass spectrometry (SIMS) and mass increase, the transverse profile determined from a model that integrates the OPD from PSDI, the topography shape, and the density and refractive index from the ellipsometry.

The primary diagnostic for this study is the Omega High Resolution Velocimeter (OHRV), a two-dimensional velocity interferometer with spatial resolution of ~5 um and velocity resolution of <10 m/s [28]. The two-dimensional velocity maps obtained with this diagnostic provide a measurement of the spatial velocity nonuniformity at the shock front which is representative of the heterogeneity in the ablation front. Recent improvements to the diagnostic reduced the velocity detection limit to 4 m/s rms Shock breakout times are determined using a streaked optical pyrometer (SOP) which collects the thermal emission at 400 nm as a function of time. Timing fiducials from the facility and the OHRV probe laser provide the timing of the OHRV probe relative to the transit of the shock from the GDP to the PMMA.

The OHRV directs a pair of 2-ps-duration probe pulses onto the shock front, separated by a known time interval, typically 160 ps. The instrument then combines the returned pulse pair interferometrically to produce a fringe pattern that provides a spatially-resolved map of relative

velocity perturbation over the field of view. Times quoted below are the centroid of the two interfered probe pulses.

The effect of the drive-side oxygen modulations is immediately apparent in the velocity maps obtained from analysis of the OHRV data, shown for three different OHRV probe times in Fig. 2. In all cases a dominant 100 µm modulation is clearly visible. At the latest probe time in the figure, 3.70 ns, the perturbation appears to be a single-mode, without obvious harmonic content, while the velocity maps for the two earlier times exhibit observable higher harmonics consistent with the initial perturbation, Fig. 1(b) and (c).

The time dependence of the perturbation was investigated with a series of experiments at different OHRV probe delays. Profiles from six shots with different OHRV delays are shown in Fig. 3. The GDP thickness was 50 µm for times 3.48 ns and later, and 35 µm for earlier times, in order to move the breakout time from the GDP into the PMMA earlier. The average shock speed based on shock transit times is 19 ± 1.5 km/s. The GDP and PMMA are closely matched in acoustic impedance and in simulations the evolution of the perturbed shock does not depend on GDP thickness. The perturbation evolves in time as a damped oscillation with a time period $\approx 2\lambda/c_s$, where c_s is the sound speed behind the shock, roughly the shock speed. As expected [31], the higher harmonic perturbations at 50 and 33 µm decay more rapidly than the 100 µm perturbation, which persists 4 ns after the laser drive turns on.

The shock front can acquire perturbations in a variety of ways. A topographic feature on either surface launches the Richtmyer-Meshkov instability at that surface, with a corresponding feature on the shock front [32,33]. An inhomogeneity in density or composition induces a ripple on the shock [34]. A region of additional oxygen near the ablation side acts both via higher density and higher opacity to cause modulations to the pressure generated by the x-ray drive. As the shock propagate through the ablator it can acquire additional perturbations from any inhomogeneity in that material [34]. Similarly, an initially nonuniform shock undergoes damped oscillations as described in detail by Bates or Miller & Ahrens [31,35].

In the case of the imposed oxygen profiles shown in Fig. 1(c), simulations indicate that the shock launched in the more oxygenated material lags that in the less oxygenated material by about 0.15 µm after a distance of 15 microns. The observed velocity modulation is smaller than might be expected from this amplitude modulation because the shock perturbation decays during propagation before it is measured. The shock is observed during subsequent oscillatory decay and the perturbation harmonics evolve independently, in a manner that is consistent with existing

theory [31,35], and described in detail by simulations. The comparison of simulations with the experiments is shown in Fig. 4. The agreement is generally good for all harmonics of the initial perturbation.

Photo-oxidation of GDP can be mitigated and experiments were done to test one scheme: deposition of a 20-nm thick surface layer of Al_2O_3 via atomic layer deposition (ALD) [36]. Experiments identical to the above were done with ALD-coated GDP foils, including masked light exposure of the ALD-coated foil. OHRV on these foils showed no visible features with the 100 μm imposed modulation, and an overall rms velocity of 24 m/s. Also, experiments were done using GDP control foils not intentionally exposed and protected from incidental light exposure. On these foils the OHRV also returned featureless data with rms 6 m/s. ALD-coated GDP that was not intentionally exposed to light returned featureless OHRV data with rms 9 m/s. Hence, mitigation with ALD was completely successful; integrating this into the fabrication process for cryogenic GDP NIF capsules remains in active development.

While significant work has been done to eliminate surface features from the ICF capsule materials, the significance of internal heterogeneities as discussed here is still being quantified. These experiments validate simulations indicating that internal chemical variations within the ablator can provide a significant seed for the instabilities that degrade capsule performance. The magnitude of the velocity perturbation from photoinduced heterogenous oxygenation agrees well with simulations performed by Haan et al. [18], strengthening the argument that an important instability seed in GDP shells is heterogenous oxygen distribution which most likely results from light exposure during metrology and the use of UV-curing adhesives during assembly. Radially integrated oxygen modulations of order 1 at%-μm as considered here are also estimated to be present in NIF shells, largely because of photo-oxidation, as discussed in refs. 18 and 22. The experiments described here are in agreement with simulations of the evolution of the velocity amplitudes of the relevant wavelengths. These simulations indicate that the corresponding vorticity seeds substantial instability growth in NIF implosions.
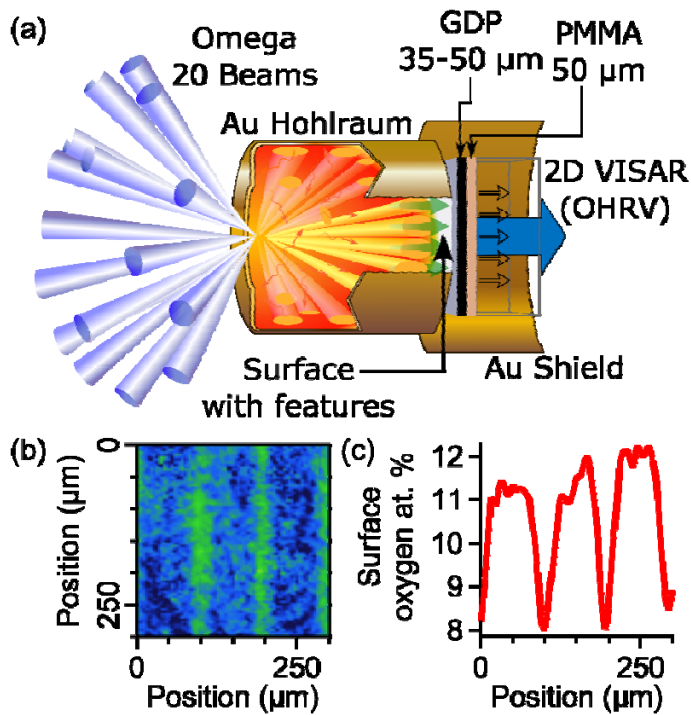
FIG. 1. (a) Target schematic for the halfraum-drive GDP targets. GDP is opaque to 400 nm probe wavelength and the detection medium is PMMA as shocks stronger than 1 Mbar are optically reflecting in the PMMA. (b) Characteristic oxygen atomic percent over a subset of the GDP foil. (c) Line profile integrated over the vertical span of (b) showing additional structure on the peaks.
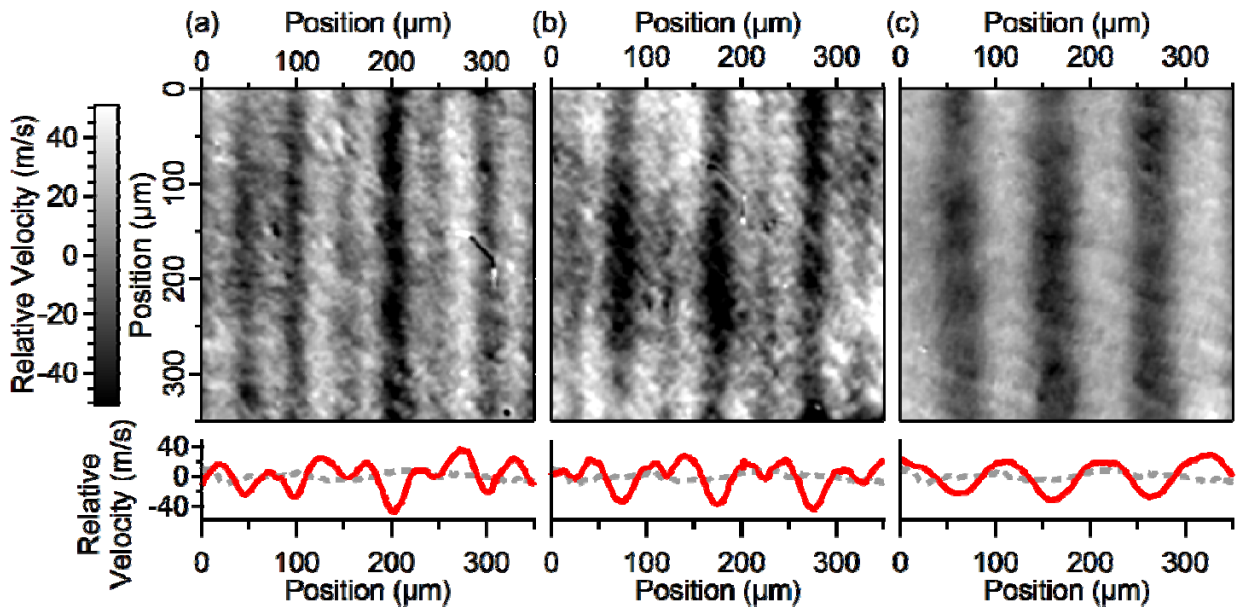
FIG. 2. Velocity map and horizontal line profile from x-ray driven light-exposed GDP foils at (a) 2.50 ns, (b) 2.80 ns, and (c) 3.70 ns after drive arrival. The horizontal line profiles shown on the

bottom are vertically averaged over the span of the velocity maps shown and the dashed, grey line is a profile from a non-patterned, driven sample.
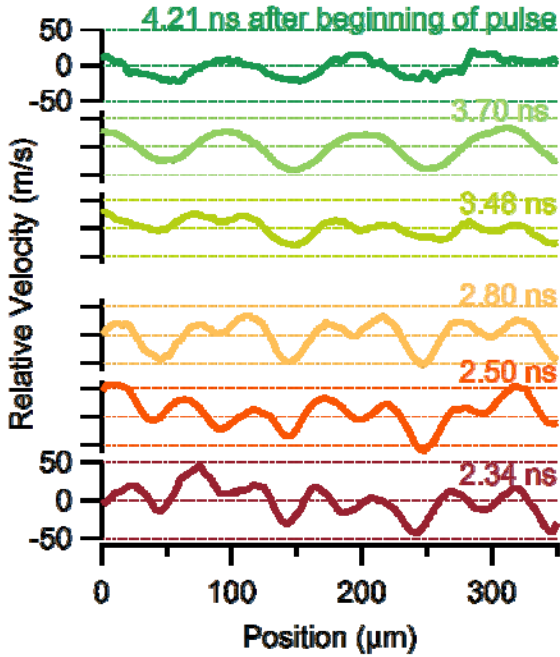
FIG. 3. Temporal evolution of the 100 μm perturbation. Each profile is plotted on separate, identical axes. Indicated time is relative to the drive beam.
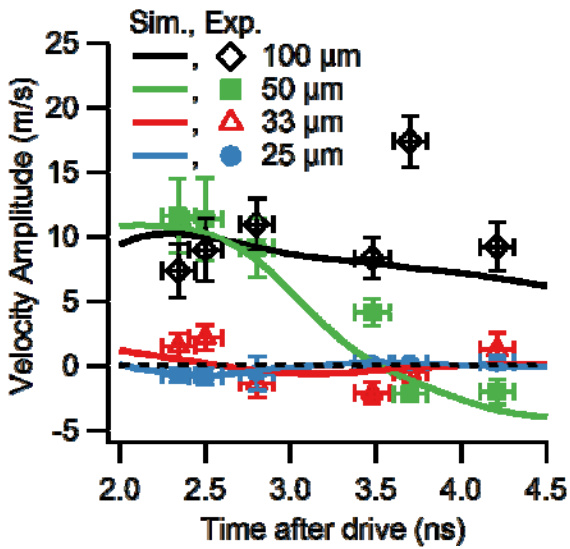
FIG. 4. Temporal evolution of the velocity amplitude for the three harmonics observed in the data.

[1]   J. Lindl, Phys Plasmas **2**, 3933 (1995).
[2]   O. A. Hurricane *et al.*, Nature **506**, 343 (2014).
[3]   G. H. Miller, E. I. Moses, and C. R. Wuest, Opt Eng **43**, 2841 (2004).
[4]   D. C. Wilson *et al.*, Phys Plasmas **5**, 1953 (1998).
[5]   J. Biener *et al.*, Nucl Fusion **49** (2009).
[6]   A. Nikroo and J. M. Pontelandolfo, Fusion Technol **38**, 58 (2000).
[7]   S. W. Haan *et al.*, Phys Plasmas **18** (2011).
[8]   V. A. Smalyuk *et al.*, Phys Rev Lett **112** (2014).
[9]   V. A. Smalyuk *et al.*, Phys Plasmas **21** (2014).
[10]   J. Melvin, H. Lim, V. Rana, B. Cheng, J. Glimm, D. H. Sharp, and D. C. Wilson, Phys Plasmas **22**, 022708 (2015).
[11]   E. I. Moses and C. R. Wuest, Fusion Sci Technol **47**, 314 (2005).
[12]   D. S. Clark *et al.*, Phys Plasmas **23** (2016).
[13]   V. A. Smalyuk *et al.*, Phys Plasmas **22**, 072704 (2015).
[14]   R. Tommasini *et al.*, Phys Plasmas **22**, 056315 (2015).
[15]   S. R. Nagel *et al.*, Phys Plasmas **22**, 022704 (2015).
[16]   A. G. MacPhee *et al.*, Phys Rev E **95**, 031204 (2017).
[17]   V. A. Smalyuk *et al.*, 9th International Conference on Inertial Fusion Sciences and Applications (Ifsa 2015) **717** (2016).
[18]   S. W. Haan, H. Huang, M. A. Johnson, M. Stadermann, S. Baxamusa, S. Bhandarkar, D. S. Clark, V. Smalyuk, and H. F. Robey, Phys Plasmas **22** (2015).
[19]   T. R. Dittrich *et al.*, 9th International Conference on Inertial Fusion Sciences and Applications (Ifsa 2015) **717** (2016).
[20]   A. J. MacKinnon *et al.*, Phys Plasmas **21**, 056318 (2014).
[21]   N. M. Hoffman and D. C. Swift, Shock Compression of Condensed Matter - 2003, Pts 1 and 2, Proceedings **706**, 1339 (2004).
[22]   E. L. Alfonso, F. Y. Tsai, S. H. Chen, R. Q. Gram, and D. R. Harding, Fusion Technol **35**, 131 (1999).
[23]   V. A. Smalyuk *et al.*, 8th International Conference on Inertial Fusion Sciences and Applications (Ifsa 2013) **688** (2016).
[24]   S. Baxamusa, T. Laurence, M. Worthington, and P. Ehrmann, Polym Degrad Stabil **122**, 133 (2015).
[25]   H. Huang, D. M. Haas, Y. T. Lee, J. J. Wu, K. A. Moreno, R. B. Stephens, A. Nikroo, M. Stadermann, and S. D. Bhandarkar, Fusion Sci Technol **63**, 142 (2013).
[26]   T. R. Boehly *et al.*, Rev. Sci. Instrum. **66**, 508 (1995).
[27]   H. Reynolds, S. Baxamusa, S. W. Haan, P. Fitzsimmons, L. Carlson, M. Farrell, A. Nikroo, and B. J. Watson, Journal of Applied Physics **119** (2016).
[28]   P. M. Celliers, D. J. Erskine, C. M. Sorce, D. G. Braun, O. L. Landen, and G. W. Collins, Rev Sci Instrum **81**, 035101 (2010).
[29]   H. Medecki, E. Tejnil, K. A. Goldberg, and J. Bokor, Opt Lett **21**, 1526 (1996).
[30]   G. E. Sommargren, D. W. Phillion, M. A. Johnson, N. Q. Nguyen, A. Barty, F. J. Snell, D. R. Dillon, and L. S. Bradsher, in *SPIE's 27th Annual International Symposium on Microlithography* (SPIE, 2002), p. 13.
[31]   J. W. Bates, Phys Rev E **69** (2004).
[32]   V. N. Goncharov, Scot Grad Ser, 419 (2009).
[33]   V. N. Goncharov, P. McKenty, S. Skupsky, R. Betti, R. L. McCrory, and C. Cherfils-Clerouin, Phys Plasmas **7**, 5118 (2000).
[34]   D. H. Munro, Phys Fluids B-Plasma **1**, 134 (1989).
[35]   G. H. Miller and T. J. Ahrens, Rev Mod Phys **63**, 919 (1991).
[36]   M. D. Groner, S. M. George, R. S. McLean, and P. F. Carcia, Appl. Phys. Lett. **88**, 051907 (2006).